



HAL
open science

Influence of moisture and drying on fatigue damage mechanisms in a woven hemp/epoxy composite: Acoustic emission and micro-CT analysis

R. Barbière, F. Touchard, L. Chocinski-Arnault, D. Mellier

► **To cite this version:**

R. Barbière, F. Touchard, L. Chocinski-Arnault, D. Mellier. Influence of moisture and drying on fatigue damage mechanisms in a woven hemp/epoxy composite: Acoustic emission and micro-CT analysis. *International Journal of Fatigue*, 2020, 136, pp.105593. 10.1016/j.ijfatigue.2020.105593 . hal-03008479

HAL Id: hal-03008479

<https://hal.science/hal-03008479>

Submitted on 16 Nov 2020

HAL is a multi-disciplinary open access archive for the deposit and dissemination of scientific research documents, whether they are published or not. The documents may come from teaching and research institutions in France or abroad, or from public or private research centers.

L'archive ouverte pluridisciplinaire **HAL**, est destinée au dépôt et à la diffusion de documents scientifiques de niveau recherche, publiés ou non, émanant des établissements d'enseignement et de recherche français ou étrangers, des laboratoires publics ou privés.

Influence of moisture and drying on fatigue damage mechanisms in a woven hemp/epoxy composite: acoustic emission and micro-CT analysis.

R. Barbère, F. Touchard, L. Chocinski-Arnault, D. Mellier

Département Physique et Mécanique des Matériaux, Institut Pprime

CNRS-ENSMA-Université de Poitiers UPR 3346, ISAE-ENSMA

1 Avenue Clément Ader, 86961 Chasseneuil, France

romain.barbiere@ensma.fr

fabienne.touchard@ensma.fr

laurence.chocinski@ensma.fr

david.mellier@ensma.fr

ABSTRACT: For the last 20 years, plant fibres have emerged as an alternative to glass fibres in composites. However, a crucial issue with plant fibre composites is their durability, i.e. their long-term hygrothermal and fatigue performances. This study deals with the influence of different conditionings (Ambient, Wet and Wet/dry) on the fatigue behaviour of $[(\pm 45)]_7$ hemp/epoxy composites. The induced damage mechanisms are investigated by acoustic emission and micro-CT. Results show that the Wet samples exhibit the lowest fatigue sensitivity despite their greatest damage quantity, whereas the Wet/dry specimens behave like pre-damaged Ambient ones. Micro-CT scans show that the same type of damage appears in all cases: cracks are made of a coalescence of partial debondings at hemp yarn/matrix interfaces, which can lead to macro-cracks crossing the sample thickness. Moreover it is demonstrated that, during fatigue tests, the evolution of cumulative AE energy and hysteresis loop energy, and the evolution of damage quantity measured by micro-CT and final hysteresis energy, are very similar whatever the conditioning.

Keywords: Environmental effects, Damage, Acoustic emission, Polymer matrix composites.

1. Introduction

Composite materials take a key place in the transport field due to their high specific strength and stiffness. Today, 95% in volume of the used composites are reinforced with glass fibres [1]. But these fibres are non-recyclable and very high energy-consuming to produce. In this context, natural fibres, such as plant fibres, have emerged as a lightweight, low cost and comparable property-wise alternative to glass fibre in composites [2–7]. However, the expansion of these materials is inhibited by a lack of knowledge of their durability, i.e. of their long-term hygrothermal and fatigue performance [8–10]. Fatigue-related mechanisms are responsible for many, if not most, failures in engineering structures where dynamic repetitive loading at levels lower than ultimate strengths still results in sudden and catastrophic failure due to internal damage accumulation over a period of time. The fatigue life is thus an essential aspect of characterising plant fibre composites (PFCs). There are some studies dealing with the fatigue behaviour in ambient environment of PFCs with short fibres [11,12], with non-woven fibres [13,14], or with long fibres [15,16]. In particular, Liang et al. have shown that, for the same lay-up, the flax composites have a lower reduction in fatigue life in comparison to glass/epoxy [17].

Concerning the PFC water sensitivity, the hydrophilic behaviour of plant fibres induces a decrease in the interfacial characteristics compared to the glass fibre composites [18]. Indeed, plant fibres are mainly composed of four

constituents: cellulose, hemicellulose, pectin and lignin. Cellulose, which is semi-crystalline polysaccharide, is the main component, leading to the excellent structural properties of plant fibres, but also responsible for their hydrophilic characteristics [19]. The water absorption and its consequences on tensile characteristics have been already widely studied for PFCs [20–22], and all studies show a decrease in strength and rigidity due to moisture effect. In a previous study, it has been shown that damage occurs in PFCs during the drying, after the water absorption [23]. Therefore, it is a crucial issue to analyse the fatigue behaviour of these materials in Wet and Wet/dry conditions. In the present work, a woven hemp/epoxy composite is studied and the fatigue behaviour of this type of composites in different moisture environments has yet to be investigated.

In order to deeply analyse fatigue damage mechanisms, two different techniques are used: acoustic emission and micro-CT. Acoustic Emission (AE) has already been successfully applied in order to locate and monitor damage evolution in a variety of composite materials. It can be used to identify damage mechanisms with the assumption that each type of damage generates AE signals with specific features [24–26]. X-ray micro-CT with high resolution allows quantitative measurements in three dimensions. Only few studies deal with the use of X-ray micro-CT on plant fibre composites, for example for the measurement of orientation and dimension of short fibres in composites [27], or for damage quantification in woven PFC [28].

The objective of this work is to study the effect of water ageing and drying on fatigue behaviour of a $[(\pm 45)]_7$ woven hemp/epoxy composite and to analyse the relation between fatigue life and damage mechanisms.

2. Materials and methods

2.1 Tested materials

The composite of this study is constituted of seven plies of plain woven hemp fabric impregnated with epoxy resin. The hemp fabric has an areal weight of $290 \pm 10 \text{ g/m}^2$. The epoxy resin is an EPOLAM 2020 from Axson Technologies with a density of 1.10 g/cm^3 . The hemp fabric was pre-dried at 40°C for 24h and the composite plates were manufactured by vacuum infusion. The composite plates were cured with the following cycle: 24h at ambient temperature, 3h at 40°C , 2h at 60°C , 2h at 80°C and 4h at 100°C , to achieve a cross-linkage as complete as possible. The final glass transition temperature measured by DSC is $89 \pm 2^\circ\text{C}$. The fibre volume fraction is $40 \pm 3\%$. The stacking sequence of the studied composite plates is $[(\pm 45)]_7$, i.e. the warp direction of each ply is oriented alternately at $+45^\circ$ and -45° from the tensile axis (X axis). From these plates, rectangular specimens were cut with the dimensions of $140 \text{ mm} \times 20 \text{ mm} \times 3,6 \text{ mm}$ (Fig. 1). The jaws of test machine took 30 mm of each

specimen extremity and 80 grit sand papers were used in the jaws to improve clamping. The gauge length was 80mm.

Three conditionings were performed on these specimens in order to evaluate the influence of moisture and drying on the fatigue behaviour of the composite:

- “Ambient” samples were stored at ambient temperature and humidity (about $21 \pm 2^\circ\text{C}$ and $48 \pm 5\%$ of relative humidity (RH) respectively) and tested at ambient temperature and humidity (about $21 \pm 1^\circ\text{C}$ and $48 \pm 5\%$ RH respectively).

- “Wet” samples were immersed in water at $21 \pm 2^\circ\text{C}$ during more than 90 days and tested in a climatic chamber at $\text{RH } 97 \pm 2\%$ and $21 \pm 1^\circ\text{C}$.

- “Wet/dry” samples were immersed in water at $21 \pm 2^\circ\text{C}$ during more than 90 days and dried in an oven during 48h at 40°C , tests were performed at ambient temperature and humidity (about $21 \pm 1^\circ\text{C}$ and $48 \pm 5\%$ RH respectively).

2.2 Mechanical testing

Mechanical tests were performed by using an INSTRON 8802 hydraulic machine with 100kN load cell and an associated climatic chamber, to allow the control of temperature and hygrometry. In order to define the stress levels for fatigue testing, tensile strength values (σ_u) need to be determined. For monotonic tensile tests, the crosshead speed was fixed at 0.5mm/min and an extensometer with a 25mm gauge length was used for measuring strain values. For fatigue tests, constant amplitude loads were applied in a sinusoidal waveform at the frequency (f) of 1 Hz in order to limit self-generated heating in the specimen. Stress ratio (R), the ratio between minimum stress (σ_{\min}) and maximum stress (σ_{\max}), was equal to 0.01 for all fatigue tests. At least 8 specimens were tested for each conditioning. Section area values of samples have been measured just before each mechanical test. So the possible variations of sample dimensions due to the different environmental conditions are taken into account.

2.3 Acoustic emission

In order to obtain an *in situ* analysis of the damage process, mechanical tests were instrumented with acoustic emission (AE) monitoring. When a material is damaged, some transient elastic sound waves are emitted and can be registered by using piezoelectric sensors fixed on the material (Fig. 1). The shape and the characteristics of the AE signals are directly dependent on the local damage mechanisms. AE signals contain some features representative of the source in such a manner that direct correlation exists between the damage mechanisms and

the AE parameters. Therefore, acoustic emission events can be classified using multivariable statistical analysis techniques and then attributed to a damage mechanism in the material [29–31]. In the present study, the AE monitoring was performed by using an acquisition system PCI-2 of Mistras Group Corporation. The piezoelectric sensors were two $\mu 80$ 65mm apart with a resonance frequency of 300Hz. Each sensor was connected to a 40dB preamplifier, without jaws contact. The amplitude threshold during AE monitoring was defined at 37dB. The coupling agent used was blu tack. Each test was preceded by a data acquisition calibration step. By using a pencil lead break procedure, the acoustic wave speed was measured. Events were determined with hits that were detected by each sensor, and that were localized with the sound speed propagation along the gauge length.

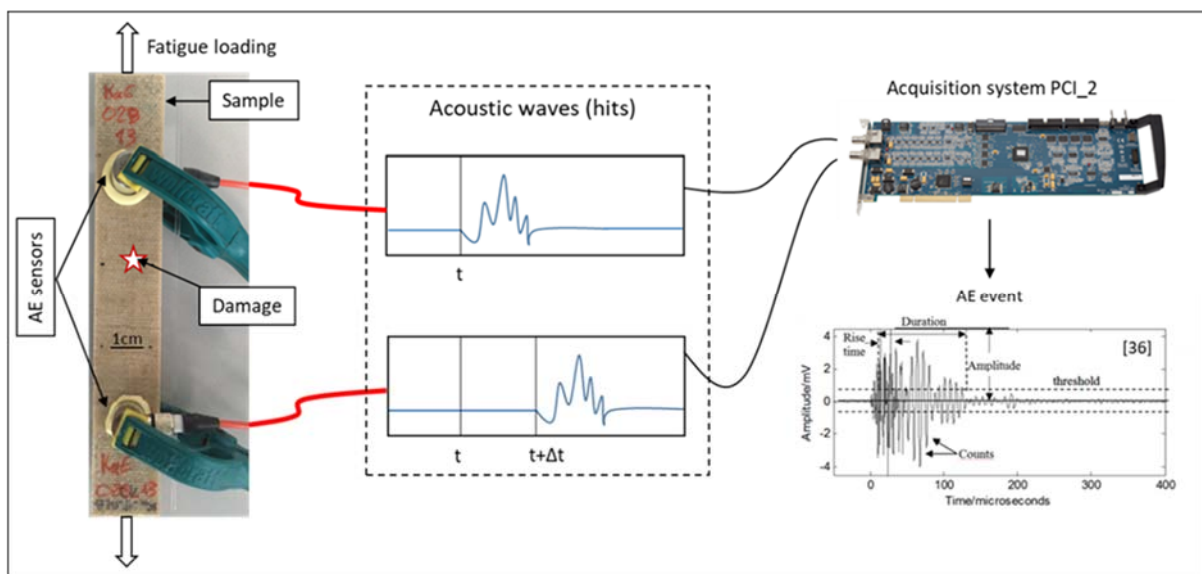


Fig. 1: Sample geometry and detection principle of the acoustic emission detection

Post-processing was done using a multi-parametric identification, based on the k-means algorithm. The k-means algorithm aims to partition data into k clusters by minimizing the euclidian distance between each value and the nearest centre [32]. This algorithm is unsupervised, which means that the number of clusters k has to be known *a priori*. It is an iterative algorithm that allocates each value to the closest centroid. In this study, data are acoustic events and five descriptors have been chosen among all AE parameters: amplitude, duration, rise time, absolute energy and number of counts (Fig. 1) [33,34]. These descriptors were preliminarily normalized and a principal component analysis (PCA) was performed. The PCA is an orthogonal linear transformation that can transform multidimensional AE data into lower dimensions with a new coordinate system, with a set of uncorrelated features, that is, the principal components. It is an effective and useful multivariate analysis method which is usually used to reduce dimensionality of a large data set to enable better analysis and visualization of data. PCA projects the input data (AE signal parameters) on the new coordinates (called principal components) with maximum variance

in the data set [35,36]. The PCA output data were submitted to the k-means algorithm. Each cluster was then associated to one damage mechanism. Studies dealing with woven composite damage process have highlighted three major damage types: matrix cracking, interface damage and fibre breakage [37–40]. Thus, it was chosen to create three clusters. Attribution of each cluster to one particular damage mechanism was done by using the form of the cluster on the radar chart [41]. It has been checked that radar charts are reproducible for tensile and fatigue tests and for the different conditionings. Therefore, they allow the attribution of each cluster to the corresponding mechanism. Fig. 2 shows two examples of radar charts obtained for Ambient and Wet samples tested in fatigue loading. The quantities in the radar charts are average relative values of the five AE event descriptors for each event cluster. The cluster with lower parameter values has been attributed to the matrix damage, the intermediate one to the interfacial damage and the last one with higher parameter values to the fibre damage.

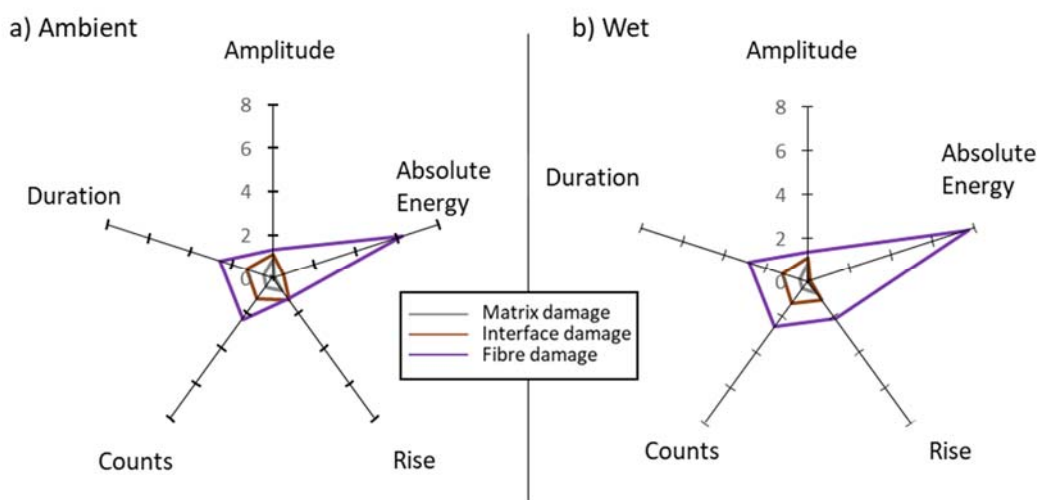


Fig. 2. Radar charts obtained for a) Ambient and b) Wet $[(\pm 45)]_7$ hemp/epoxy samples during fatigue tests with the five selected descriptors: amplitude, absolute energy, rise time, number of counts and duration.

2.4 Micro-CT

After failure, a micro-CT analysis was performed using an UltraTom CT scanner manufactured by RX Solution (France). The system consists in a Hamamatsu micro focus sealed X-ray tube operating at 20-150kV/0-500 μ A, within a maximum power of 75W. A precision object manipulator with two translations and one rotation facilitates rotating the sample for acquisition of tomographic data, and displacement along the optical axis to adjust the magnification. X-rays generated by the source diverge at an angle providing a cone-beam, thus samples can be

imaged at various geometric magnifications by moving the sample close to the source to provide high resolution mode or close to the detector to provide low resolution measurements. The generator and the detector are also mobile to cover a large range of magnification. A 15 μm resolution has been used in this work, with an accelerating voltage of 50kV and a beam current of 280 mA. The flat panel detector used in this study has 1920 pixels x 1536 pixels with a pixel size of 127 μm . This X-ray detector consists in an X-ray CsI scintillator screen which is settled on an amorphous silicon layer. The X-ray shadow projections are digitized with 65536 brightness gradations (16 bits) and recorded in TIFF format. The image acquisition time was about 2h per specimen. For 3D reconstruction, X-ray images were acquired from 1120 rotation views over 360° of rotation. The reconstruction was performed using an algorithm based on the filtered back-projection procedure for Feldkamp cone beam geometry. The analysis of the obtained volume can give quantitative information about damage in the sample (Fig. 3).

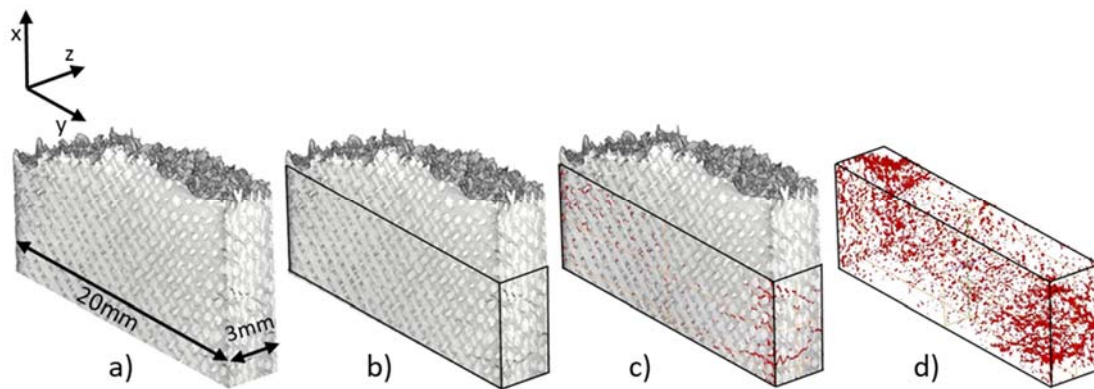


Fig. 3. Segmentation of damage process in grey level tomographs from micro-CT imaging in [(±45)]₇ hemp/epoxy sample after fatigue failure.

To this end, for each studied sample, a region of interest (ROI) was established near the failure zone but outside the fracture area (Fig. 3b). The same ROI size was chosen for all the samples. The damage was then detected by segmentation of grey levels, with a threshold for the darker voxels, which are identified as damage. It was thus possible to separate the voxels associated with damage from those attributed to the material, containing the yarns and the matrix (Fig. 3c). The last step was to isolate the voxels corresponding to damage and to quantify their volume (Fig. 3d).

3. Results and discussion

3.1 Water absorption

In order to study the effect of water ageing on fatigue behaviour, a set of samples was immersed in water at ambient temperature $21\pm 3^\circ\text{C}$. Water uptake was measured by weighing samples periodically at ambient temperature with a precision balance (precision of 0.1 mg). Relative weight gain (M_t) corresponding to the water uptake at time t is defined by Eq. 1 [42]:

$$M_t = \frac{w_t - w_i}{w_i} \times 100 \quad (1)$$

where w_t is the sample mass at t and w_i is the initial mass.

The relative weight gain was measured for 7 samples. Measurements showed good reproducibility. An example of water absorption curve, up to 800 days of immersion, is presented in Fig. 4. The water uptake increases linearly in a first step and then reaches a saturation plateau.

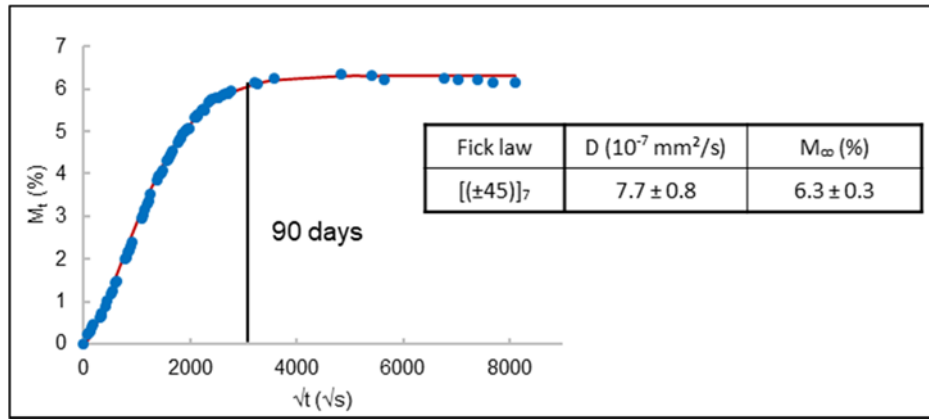


Fig. 4. Water absorption curve and Fick law for the [(±45)]₇ woven hemp/epoxy composite.

The diffusion of water in a solid is usually described by the Fick's second law of diffusion. The Fick law used here is given by Eq. 2 and 3 [42]:

$$\frac{M_t}{M_\infty} = 1 - e\left(-7.3\left(\frac{Dt}{h^2}\right)^{0.75}\right) \quad (2)$$

$$D = \pi \left(\frac{h.k}{4.M_\infty}\right)^2 \quad (3)$$

with:

M_{∞} : the water uptake at saturation,

D: the diffusion coefficient,

k: the initial slope of the M_t versus \sqrt{t} experimental curve,

h: the thickness of the specimen,

t: the time.

Experimental data have been used to determine values of the water uptake at saturation and of the diffusion coefficient. Results are given in Fig. 4. The obtained values are consistent with those given in literature for similar materials [22,43]. The superposition of the experimental and Fick's law curves confirms that the studied composite follows a Fickian behaviour (Fig. 4). These results also allow the determination of the time to reach saturation: 90 days in water are necessary to reach the plateau. Therefore, all the Wet and Wet/dry specimens used for mechanical testing were immersed in water between 90 and 100 days.

3.2 Fatigue life

3.2.1 Tensile strength

Before fatigue testing, tensile tests have been performed in order to determine the strength (σ_u) of the samples for each conditioning.

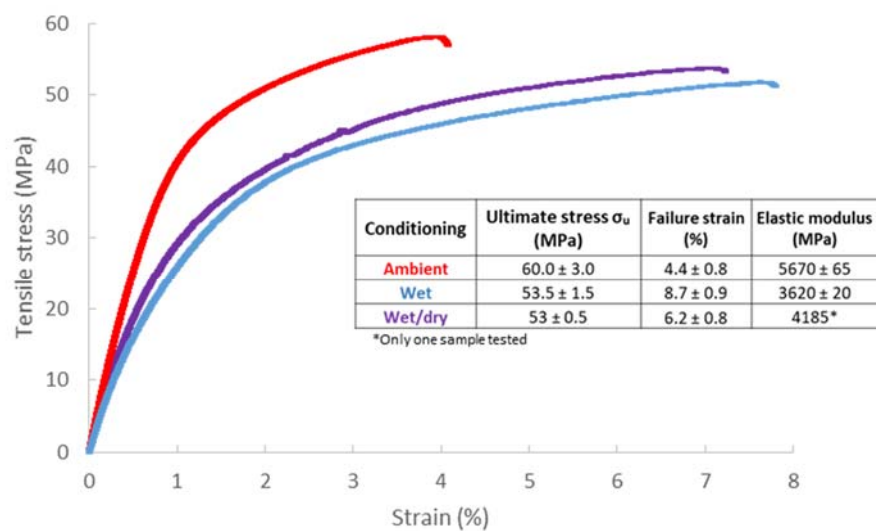


Fig. 5. Tensile tests of the $[(\pm 45)]_7$ woven hemp/epoxy composites for the three conditionings.

Fig. 5 shows tensile curves and tensile characteristic values obtained for the three conditionings. As expected, the maximum σ_u and elastic modulus E values are obtained for samples with the Ambient conditioning, i.e. for reference samples. These samples present also the smallest failure strain values. On the contrary, the Wet conditioning leads to the minimum σ_u and elastic modulus values, with a decrease of about 11% in σ_u value and 36% in E value comparatively to the Ambient conditioning. Samples with Wet conditioning show a failure strain value twice as high as the Ambient sample one (about 8.7%). These results are in accordance with other studies on similar materials [44,45]. This behaviour modification after water ageing can be linked to the plasticizing effect of the water on the polymer matrix and the reinforcement degradation. Concerning Wet/dry samples, Fig. 5 shows that σ_u value is the same as for the Wet sample one. It demonstrates that the drying step of the conditioning doesn't affect the ultimate tensile stress. But, at the same time, it has to be noted that the Wet/dry samples partially recover the stiffness and the failure strain values of the Ambient ones, but not totally. These results can be explained by the interfacial damage created during the water desorption, as it has been shown in a previous study [28].

From these tensile tests, three levels of maximum stress were chosen for fatigue tests: 60%, 75% and 90% of the tensile strength for each conditioning.

3.2.2 Wöhler curves

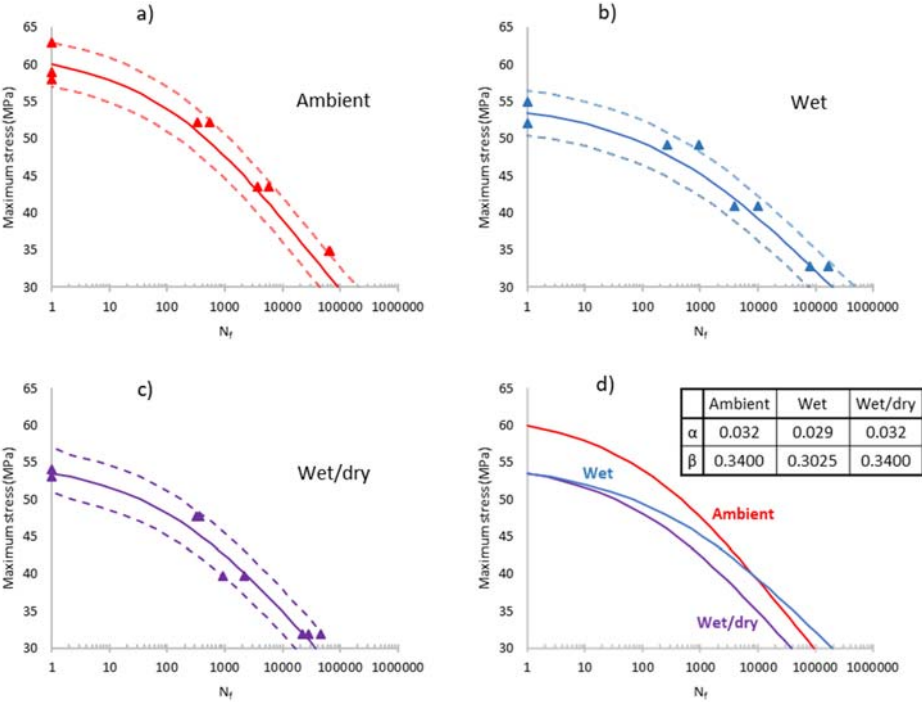


Fig. 6. Influence on fatigue life of the conditioning of [(±45)₇] woven hemp/epoxy composites: a) Ambient, b) Wet, c) Wet/dry and d) the different Epaarachchi model curves and associated parameters.

Fatigue tests were performed on $[(\pm 45)]_7$ woven hemp/epoxy composites for each maximum stress level and each conditioning. In Fig. 6, S-N curves for fatigue tests results are presented: the logarithm of the number of fatigue cycles to failure is plotted as a function of the applied maximum stress σ_{max} . For each studied stress level, there is a slight and usual dispersion in fatigue lifetime. For all the conditionings, Wöhler curves present a gradual decline in fatigue failure cycles with increasing fatigue stress level. The Ambient conditioning curve starts from a higher value of stress than the other ones due to its higher tensile strength.

Several models for fatigue life prediction of composite materials are proposed in literature [46–50]. The fatigue life model used in this study is the Epaarachchi model (Eq. 4) [51]: this model allows the prediction of the fatigue life using a very limited amount of experimental data.

$$N_f = \left[1 + \left(\frac{\sigma_u}{\sigma_{max}} - 1 \right) \frac{f^\beta}{\alpha(1-R)^{1.6-R|\sin\theta|}} \left(\frac{\sigma_u}{\sigma_{max}} \right)^{0.6-R|\sin\theta|} \right]^{\frac{1}{\beta}} \quad (4)$$

with:

N_f : the number of fatigue cycles to failure,

σ_{max} : the maximum fatigue stress,

σ_u : the ultimate tensile stress,

f : the fatigue frequency,

R : the stress ratio,

θ : the smallest angle of fibres between the loading axis and the fibre direction (45° in this study),

α and β : the only two phenomenological parameters that need to be determined from experimental data.

For this model, only one S-N curve for a given stress ratio, frequency and lay-up is necessary to obtain the α and β parameters. Therefore, α and β have been determined for each conditioning. The solid lines in Fig. 6 represent Epaarachchi fatigue behaviour model, and the dashed lines represent the dispersion of the model, based on the hypothesis that the dispersion in fatigue life is only due to the variability in static strength [52,53]. The comparison of experimental and calculated S-N curves in Fig. 6a,b,c shows the ability of the model to describe the fatigue behaviour of the material for the different conditionings. The model estimates quite well the fatigue life of the material in all cases. Fig. 6d shows the fatigue lives calculated for each conditioning and the corresponding α and β parameters. It is worth noting that the Ambient and Wet/dry samples have the same material constants α and β , which highlights that the two types of conditioning lead to the same fatigue sensitivity. The difference in their fatigue behaviour comes from the 10% decrease in the σ_u value between the Ambient and the Wet/dry

conditionings. On the contrary, different α and β parameters have been determined for the Wet conditioning samples. Indeed, this conditioning leads to a higher fatigue resistance than the one obtained for the other conditionings. Finally, these results show that, for a high σ_{\max} value, the fatigue life is higher for the Ambient conditioning than for the Wet or the Wet/dry ones, but for a low σ_{\max} value, the fatigue life is higher for the Wet conditioning than for the Ambient or the Wet/dry ones. This lower fatigue sensitivity for specimens tested in humid environment compared to the one of specimens tested in ambient conditions has also recently been shown for unidirectional flax/epoxy composite [54]. In the present study, it is also demonstrated that the Wet/dry conditioning exhibits a specific behaviour, with the same fatigue sensitivity as the one of Ambient samples and the same tensile strength as the one of Wet samples. In order to better understand these phenomena, an in-depth analysis of damage and deformation mechanisms occurring during fatigue tests in the studied woven hemp/epoxy composite for the three conditionings is presented in next sections.

3.2.3 Evolution of the mechanical parameters

During fatigue tests, the crosshead displacement and the applied loading have been recorded with a frequency of 100Hz. It has allowed to determine three mechanical parameters at each cycle: the normalized secant modulus, the maximum strain and the hysteresis loop energy. The normalized secant modulus is determined as the ratio of the slope of each hysteresis loop (Fig. 7a) by the one of the first established cycle, which corresponds to the tenth cycle for all cases. The maximum strain value is taken at the top of each hysteresis loop (Fig. 7a), and the hysteresis loop energy is given by the hysteresis loop area (Fig. 10a). The area of each hysteresis loop has been calculated as being the area of the corresponding 99-sided polygon. The evolution of the normalized secant modulus versus the normalized number of cycles is shown in Fig. 7. Three zones in the evolution of the secant modulus can be determined from Fig. 7, as already shown for different composites [15,55,56]: zone I is characterized by a significant initial slope at the beginning of the curves, then zone II shows a constant or quasi linear zone. Finally, zone III is described as the phase just before the failure and is defined by a gradually decreasing slope. It can be seen in Fig. 7 that, for all the stress levels, the decrease in secant modulus is more rapid and pronounced for the Wet conditioning than for the others. For $\sigma_{\max} = 0.6\sigma_u$, the Wet conditioning leads, at the end of the fatigue test, to a decrease in secant modulus of 55%, whereas it reaches 25% for the Ambient one (Fig. 7d). This result highlights the great sensitivity to water of plant fibre composites. Concerning the Wet/dry conditioning, for the first fatigue level $\sigma_{\max} = 0.9\sigma_u$ there is no main difference with the Ambient conditioning (Fig. 7b). At $\sigma_{\max} = 0.75\sigma_u$ (Fig. 7c) and $\sigma_{\max} = 0.9\sigma_u$ (Fig. 7d), the Wet/dry conditioning shows an intermediate behaviour between the Ambient and the Wet ones. For example, at the lowest level of fatigue (Fig. 7d), the decrease in secant modulus is of 45% at the

end of the fatigue test for the Wet/dry conditioning. It confirms that Wet/dry samples can recover only partially the behaviour of Ambient ones.

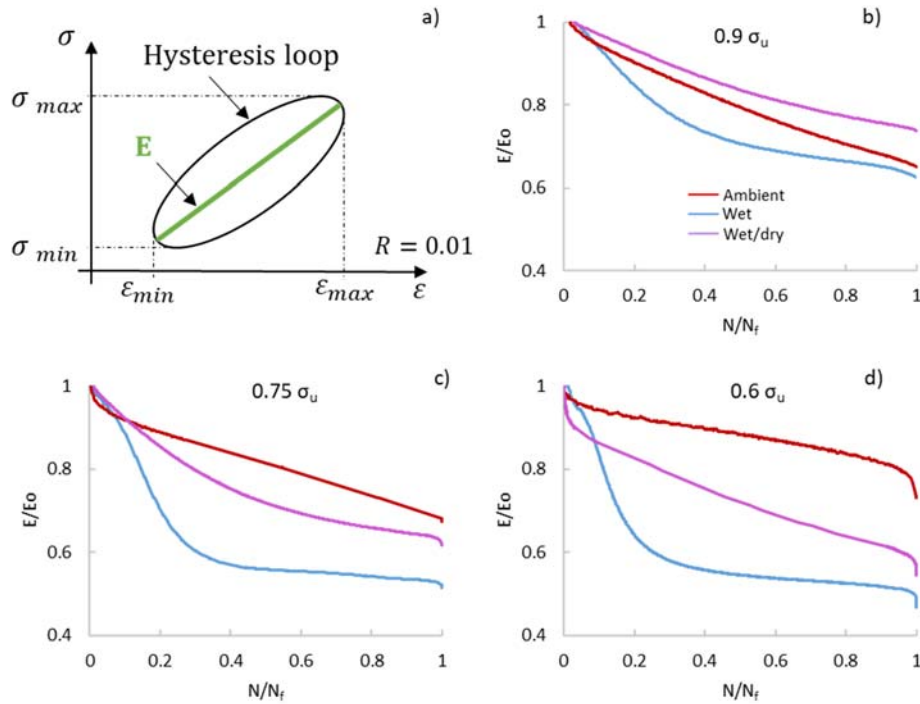


Fig. 7. a) Schematic representation for secant modulus determination. Evolution of the normalized secant modulus vs the normalized number of fatigue cycles for each conditioning and each level of maximum fatigue stress: b) for $\sigma_{max} = 0.9\sigma_u$, c) for $\sigma_{max} = 0.75\sigma_u$ and d) for $\sigma_{max} = 0.6\sigma_u$.

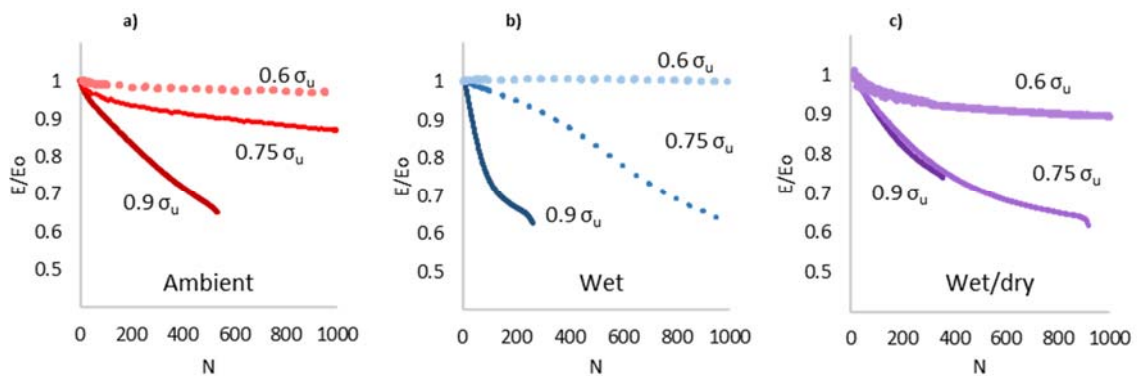


Fig. 8. Evolution of normalized secant modulus during the first thousand fatigue cycles for each level of maximum fatigue stress and each conditioning: a) Ambient, b) Wet and c) Wet/dry.

The representation of the evolution of secant modulus during the first fatigue cycles allows the comparison of the damage kinetics for the different maximum stress levels (Fig. 8). It can be seen in Fig. 8 that for each conditioning, the decrease in the secant modulus is more rapid when the applied stress level increases. It can be explained by the fact that, when the applied stress increases, the damage in the composite can develop much more.

In Fig. 9 are plotted the evolutions of the maximum strain during fatigue tests at $\sigma_{max} = 0.9\sigma_u$ for each conditioning.

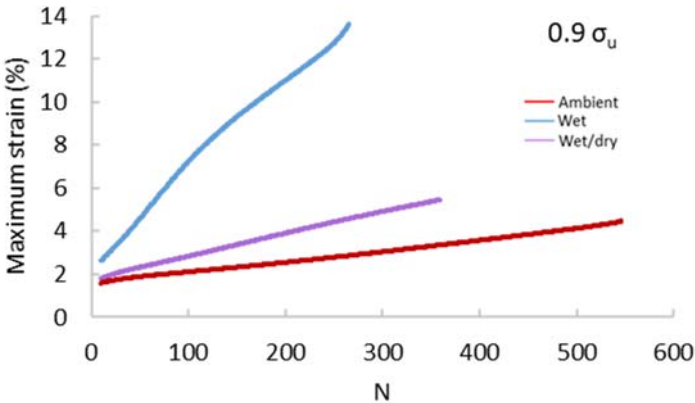


Fig. 9. Evolution of the maximum strain during fatigue tests on $[(\pm 45)]_7$ woven hemp/epoxy composites for each conditioning at $\sigma_{max} = 0.9 \sigma_u$.

As for monotonic tensile tests (Fig.5), the Wet/dry conditioning exhibits an intermediate behaviour between the Ambient and the Wet conditionings (Fig. 9). At the end of the fatigue test, the maximum strain value reaches 5.6% for the Wet/dry conditioning, whereas it reaches 4.3% for the Ambient one and 13.8% for the Wet one. This very high value for the Wet conditioning highlights the significant effect of water on both the matrix and the reinforcement in this type of composite materials.

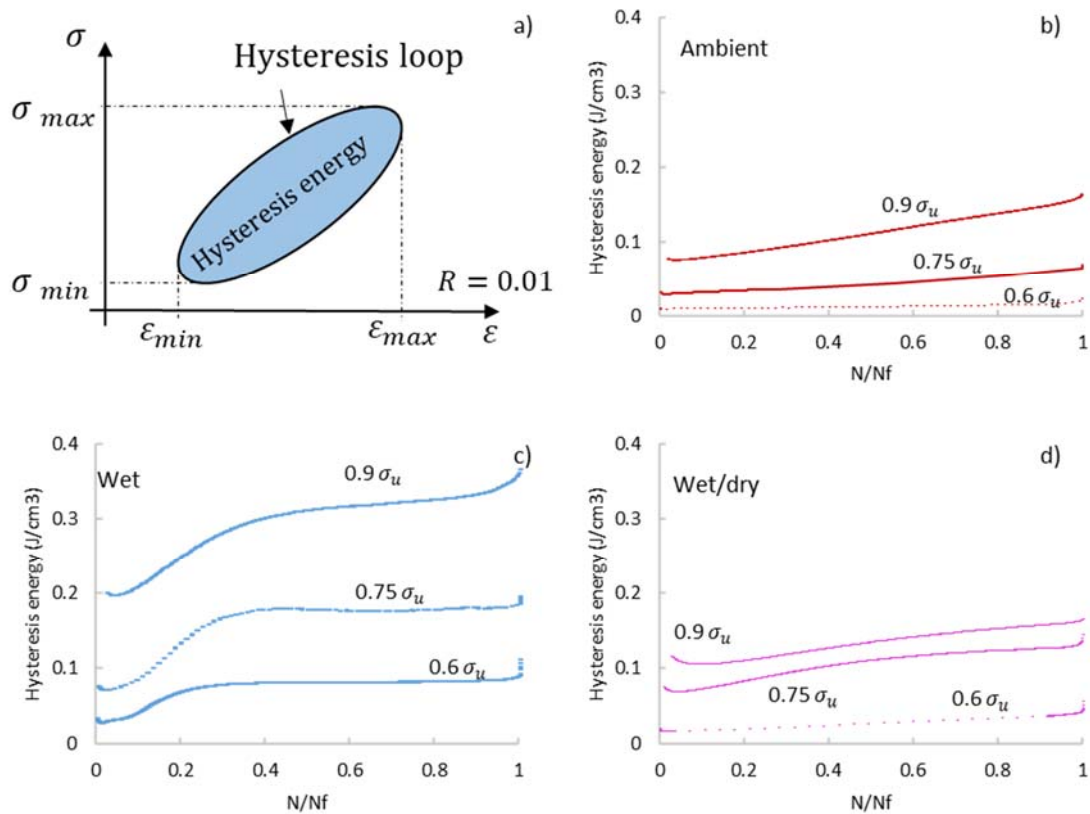


Fig. 10. a) Schematic representation of the hysteresis energy per cycle. Evolution of the hysteresis energy per cycle vs the normalized number of fatigue cycles for each level of maximum fatigue stress and each conditioning: b) Ambient, c) Wet, and d) Wet/dry.

The evolution of the area of hysteresis loops vs the normalized fatigue lifetime is presented in Fig. 10 for each σ_{max} value and each conditioning. It can be seen that, for each conditioning, the higher the applied stress, the higher the hysteresis loop area. Fig. 10 also shows that this area evolution is more than twice as high for the Wet conditioning as for the other conditionings. Moreover, the Wet conditioning exhibits a particular behaviour, with a significant increase during the first 30% of fatigue cycles. This can be explained by the fact that the hysteresis loop area corresponds with the energy dissipated in the material by several phenomena like viscosity, plasticity, self-heating and damage [57]. It confirms again that the presence of water, during the storage and during the fatigue tests, considerably modifies the behaviour of this plant fibre composite. The plasticization of the matrix and the degradation of the reinforcements and interfaces lead to dissipate more energy at each cycle of fatigue. A detailed analysis of the damage development in samples with the different conditionings has been performed to explain these different behaviours.

3.3 Damage mechanisms

3.3.1 Acoustic emission analysis

In situ damage analysis was performed by using acoustic emission during fatigue tests inside the climatic chamber. Acoustic events were recorded all along the tests and located in the gauge length of the coupon, along the loading axis. Fig. 11 shows for instance the AE events recorded during fatigue test at $\sigma_{\max} = 0.6 \sigma_u$ on a $[(\pm 45)]_7$ woven hemp/epoxy sample for the Ambient conditioning.

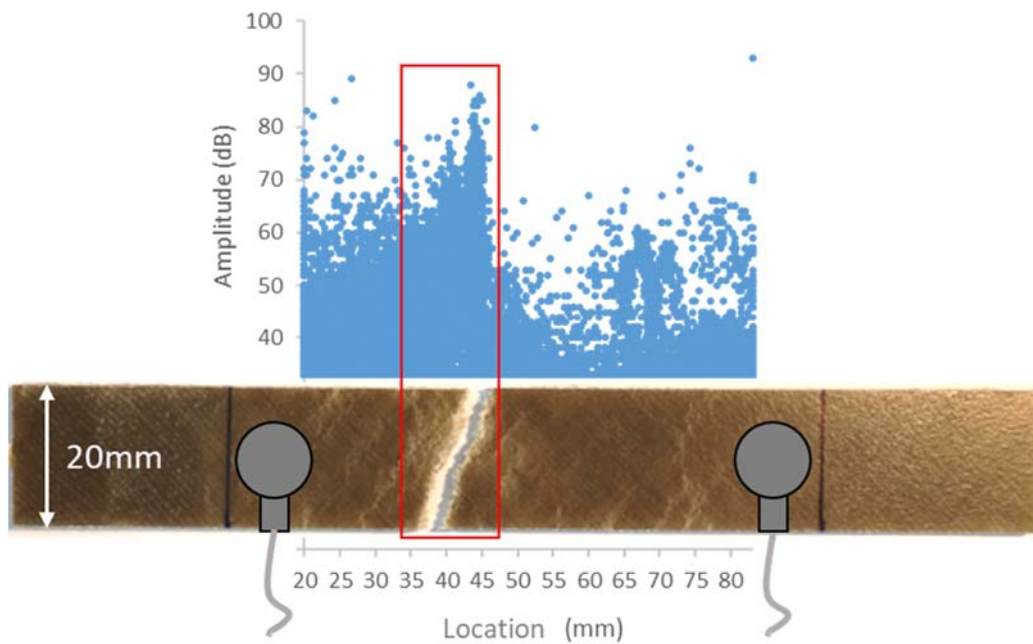


Fig. 11. Amplitude versus location of acoustic events recorded during a fatigue test at $\sigma_{\max} = 0.6 \sigma_u$ on $[(\pm 45)]_7$ woven hemp/epoxy sample for the Ambient conditioning, and comparison with the sample picture after failure.

Fig. 11 shows that acoustic events with low amplitude values are relatively well distributed along the gauge length. However, an accumulation of high amplitude events is observed at about 40mm. This position is consistent with the location of the failure. This highlights that the failure area corresponds with more numerous and high amplitude acoustic events, showing that the ultimate failure is essentially driven by fibre breakages.

The evolution of the normalized cumulative number of acoustic events during the fatigue lives of $[(\pm 45)]_7$ hemp/epoxy samples are presented in Fig. 12 for each level of applied stress and each conditioning. The normalized cumulative number of events is defined as the number of AE events until time t divided by the number of AE events until failure. It allows the comparison of the damage kinetics in specimens during fatigue tests.

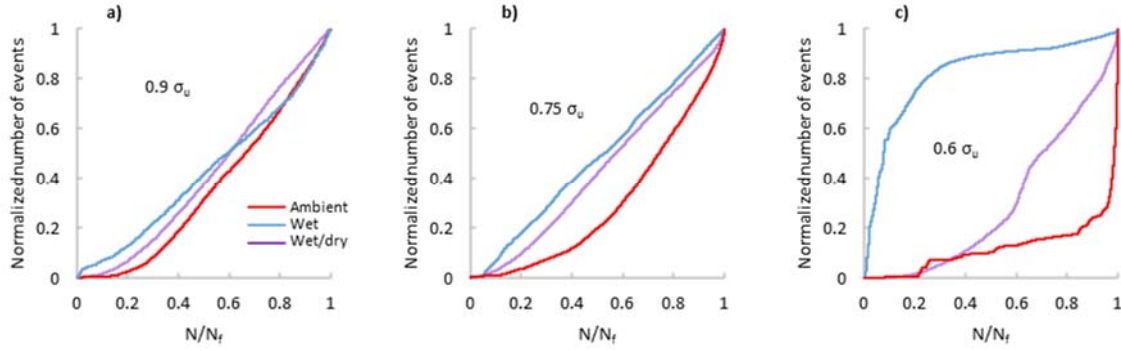


Fig. 12. Normalized cumulative number of AE events vs the normalized number of fatigue cycles for each conditioning and for the three levels of the maximum fatigue stress: a) $\sigma_{max} = 0.9 \sigma_u$, b) $\sigma_{max} = 0.75 \sigma_u$, c) $\sigma_{max} = 0.6 \sigma_u$.

Fig. 12 shows that the evolution of damage in $[(\pm 45)]_7$ woven hemp epoxy composite depends on both conditioning and stress level. For the higher stress level (Fig. 12a), the damage kinetics is similar for all the conditionings. For the intermediate stress level (Fig. 12b), the damage development in Wet and Wet/dry samples is almost the same and quite linear, whereas, for the Ambient conditioning, it grows more slowly during the first half of the fatigue test. For the lower stress level (Fig. 12c), damage kinetics are very different. In the Wet sample, there is a significant and early growth of event number and then, during the last 40% of the fatigue lifetime, very few events occur. On the opposite, in the Ambient sample, damage develops later with a gradual increase. It is only in the last 20% of the fatigue lifetime that the kinetics increases very rapidly up to failure. Finally, for the Wet/dry sample, the damage kinetics is intermediate, with a more progressive evolution during the fatigue test. These results show that differences of damage kinetics between the different conditionings are more visible for low fatigue stress level, because damage has time to develop before failure. In Figure 12c, for $\sigma_{max} = 0.6 \sigma_u$, it can be seen that for the Ambient sample, damage appears after 20% of the fatigue lifetime and develops slowly. For the Wet sample, damage grows very rapidly from the first fatigue cycles, reflecting the material degradation in presence of water. The event proportion of 85% is reached during the first quarter of the fatigue life for the Wet sample, while only few events occur at this stage for the Ambient conditioning. For the Wet/dry sample, damage appears at the same threshold as the Ambient one, but then it develops much faster - if we except last fatigue cycles just before failure. This behaviour has to be linked to the pre-damage created during the drying after the water ageing. As shown in [28], in plant fibre composites, damage appears during desorption without any applied loading. It comes from the differential shrinkage between the different constituents of the material during drying. This creates cracks at the yarn/matrix interface. It has been confirmed by investigations in single yarn composites [58]. Therefore, during

fatigue tests on Wet/dry samples, damage develops more rapidly than in Ambient specimens, because of the presence of this pre-damage.

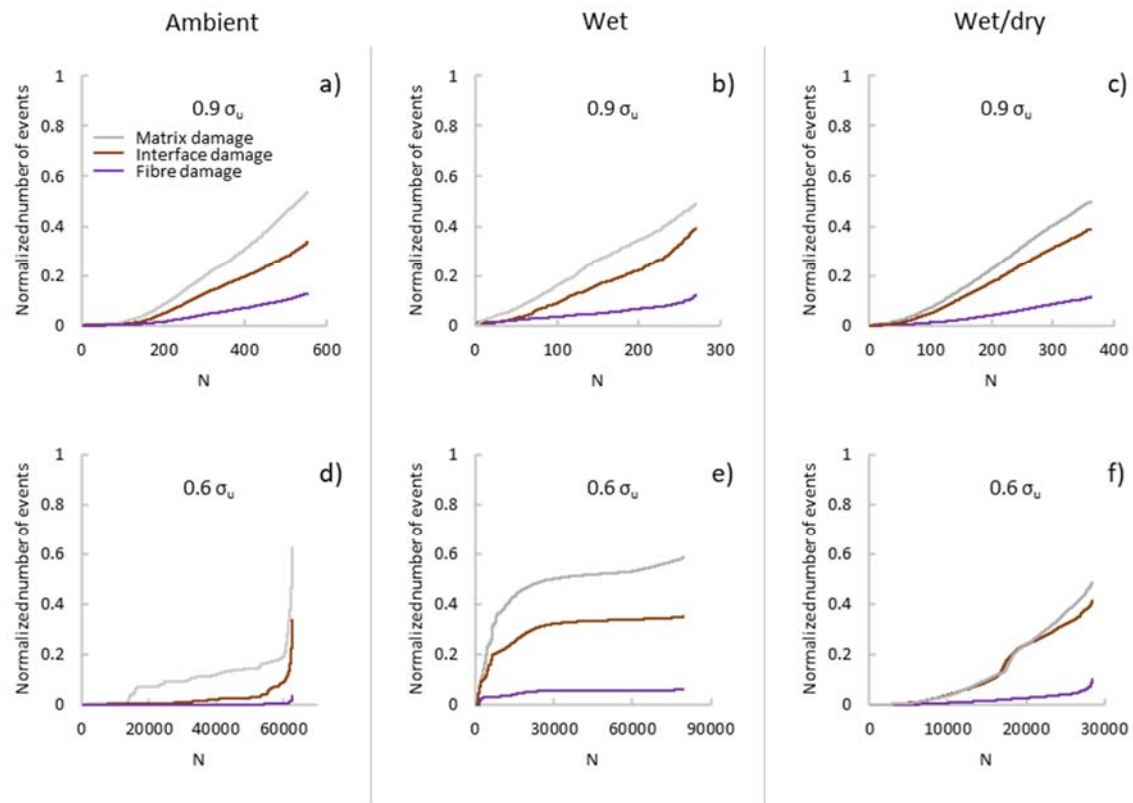


Fig. 13. Normalized cumulative number of AE events for each type of damage during fatigue tests on $[(\pm 45)_7]_7$ woven hemp epoxy composites at $\sigma_{max} = 0.9 \sigma_u$ and $\sigma_{max} = 0.6 \sigma_u$ for the three conditionings: a) and d) Ambient, b) and e) Wet, c) and f) Wet/dry.

As described in section 2.3, for all the fatigue tests, AE events have been attributed to a specific damage mechanism among matrix cracking, interface damage and fibre breakage. Fig. 13 presents results obtained for the highest and lowest stress levels, for the three conditionings. It can be seen in Fig. 13 that, in number of AE events, for all cases, matrix damage is predominant, fibre breakages are the least numerous, and interfacial damage has an intermediate evolution. For the highest stress level, $\sigma_{max} = 0.9 \sigma_u$, evolutions of the different types of damage are quite similar, whatever the conditioning (Fig. 13a,b,c). By comparing with results obtained for the lowest stress level, it can be seen that, for all the conditionings, the proportion of the reinforcement damage is higher for $\sigma_{max} = 0.9 \sigma_u$. It shows, logically, that the higher the stress level, the more the fibre breakages.

For $\sigma_{\max} = 0.6\sigma_u$, the fatigue life is more related to the matrix and interfacial damage. These mechanisms show a strong dependence on the conditioning. For the Ambient conditioning (Fig. 13d), the matrix damage occurs at the very beginning of the fatigue test, during the first quarter of the test, and interfacial damage occurs in the middle of the fatigue lifetime. The Wet conditioning shows a very early damage development for the two mechanisms (Fig. 13e), but, thanks to a higher tenacity and deformability due to the presence of water, it leads to a better fatigue lifetime at this low level of stress, as it has been seen in Fig. 6d. Concerning the Wet/dry conditioning, Fig. 13f shows a gradual increase in the matrix and interfacial damage mechanisms. The comparison of the three conditionings highlights that the Wet/dry sample presents the highest proportion of interfacial damage comparatively to the matrix one (Fig. 13d,e,f). It confirms the presence for this conditioning of a pre-damage at the yarn/matrix interface due to water desorption. All these results show that a Wet/dry sample behaves like a pre-damaged Ambient sample.

3.3.2 Micro-CT analysis

A detailed analysis of the different types of fatigue damage has been performed by realizing micro-CT scans of the hemp/epoxy composite samples after failure for the three conditionings. It allows the 3D reconstruction of the material and the observation of damage in different planes. It has to be noted that, because of the used resolution, only the defects larger than $15\mu\text{m}$ can be observed. Fig. 14 presents for instance the tomographs obtained after fatigue tests at $\sigma_{\max} = 0.9\sigma_u$ for the three conditionings. Three different planes of observation have been chosen and are described in Fig. 14a.

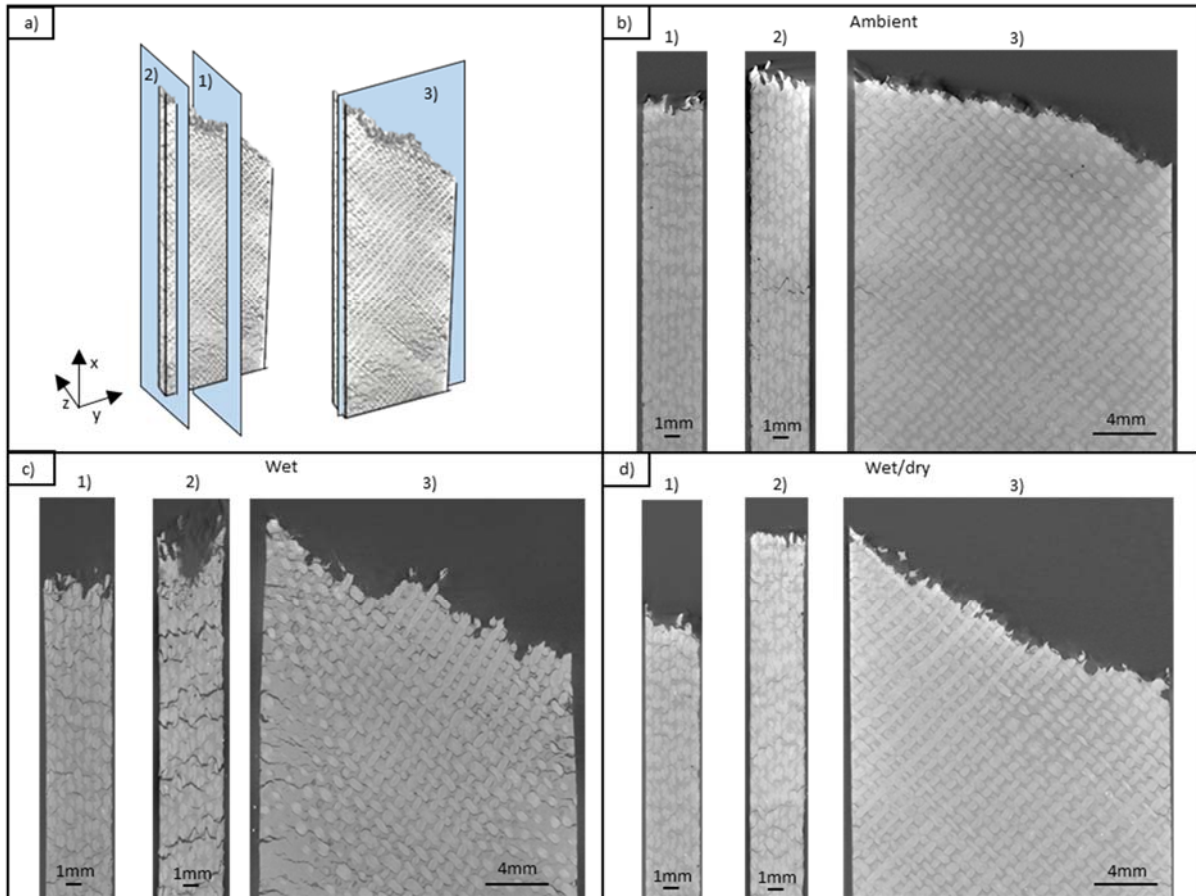


Fig. 14. Tomographs from micro-CT of $[(\pm 45)]_7$ hemp/epoxy samples after fatigue tests at $\sigma_{max} = 0.9 \sigma_u$ in three planes described in a): 1) core (ZX), 2) edge (ZX), 3) core (XY), for each conditioning: b) Ambient, c) Wet and d) Wet/dry.

The first information that can be obtained from the tomographs is the low porosity content in samples, due to the manufacturing process by vacuum infusion. The second information is given at macroscale. If we look at pictures of plane 3) in Fig. 14, we can see that the shape of the macroscopic failure is quite similar for the three conditionings. The failure starts along a yarn with a 45° angle relative to the X axis, and propagates by slipping from yarn to yarn. Then if we look at the quantity of damage, it can be seen in Fig. 14 that damage is far more developed in the sample with the Wet conditioning than in the other ones. This can be linked to the more significant decrease in secant modulus for the Wet conditioning (Fig. 7) and with its higher values of dissipated energy (Fig. 10). Fig. 14 shows also that, for all the conditionings, the damage distribution is the same: cracks are far more numerous and open at the free edges of the samples (see planes 2) in Fig. 14) and they are fewer and fewer when we move inside the material, up to obtain a quasi-undamaged area - for the applied resolution - in the core of the Ambient and the Wet/dry samples (see plane 1) in Fig. 14b and d). This is due to the well-known “free edge effect”,

which is described in literature for carbon or glass fibre composites [59,60]. For the sample with the Wet conditioning (Fig. 14c), damage is so severe that even the core of the sample is damaged (see plane 1) in Fig. 14c). For this conditioning, all the cracks cross the whole thickness of the sample (Fig. 14c-plane 2)) and their lengths reach about 7 mm, as it can be seen in Fig. 14c-plane 3). Despite the difference in damage quantity for the three conditionings, micro-CT scans show that the same type of damage appears in the three cases: cracks initiate at a yarn/matrix interface, and propagate from an interface to the next one, as it can be seen for example in Fig. 15. Each crack is made of a coalescence of partial debondings at hemp yarn/matrix interfaces, which can lead to a macro-crack crossing the sample thickness. This type of cracks has been observed in all the micro-CT scans, whatever the conditioning and the stress level. These results show that only the damage quantity is modified from one case to another, but not the damage type.

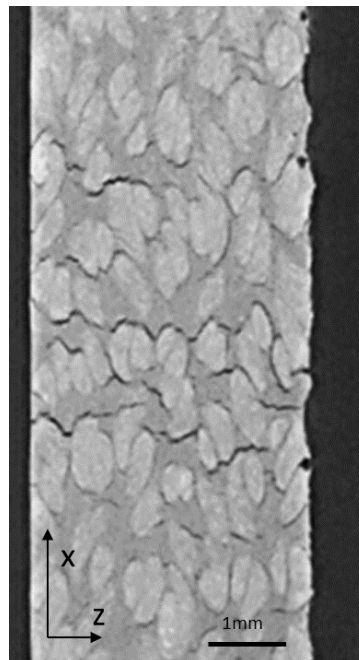


Fig. 15. Micro-CT scan in plane (ZX) for a [(±45)₇] hemp/epoxy sample after fatigue test at $\sigma_{max} = 0.9 \sigma_u$ with the Wet/dry conditioning.

3.4 Discussion

In this study, the fatigue damage evolution has been analysed by means of various techniques, each of them allowing to give different information. The objective of this section is to compare the obtained results, and thus to validate the complementarity of these methods.

3.4.1 Comparison of AE energy and mechanical energy

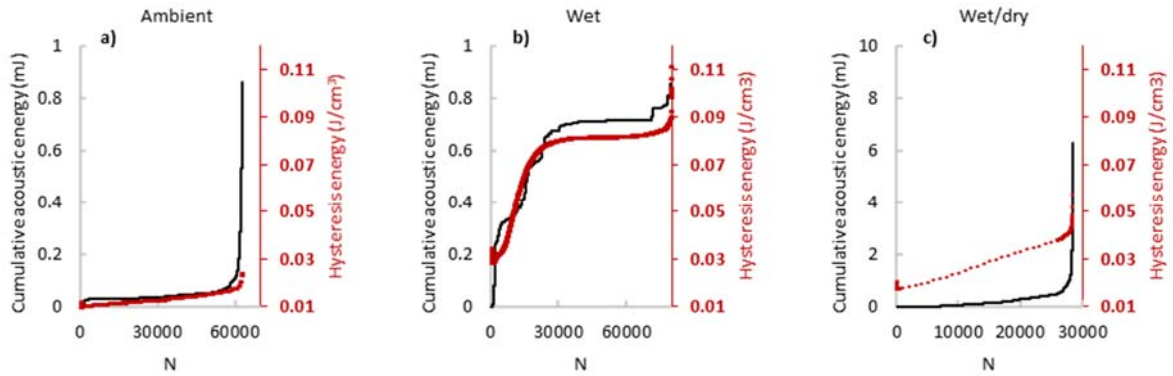


Fig. 16. Comparison of cumulative AE energy and hysteresis loop energy during fatigue tests on $[(\pm 45)]_7$ hemp/epoxy samples at $\sigma_{max} = 0.6 \sigma_u$ for each conditioning: a) Ambient, b) Wet and c) Wet/dry.

The comparison between mechanical parameters and acoustic emission data can be made through the energy. On one hand, the recording of stress and strain values during fatigue tests allows to obtain the hysteresis loop at each fatigue cycle and, thus, the energy quantity dissipated by the material. On the other hand, among the acoustic emission parameters, there is the absolute energy, which reflects the energy of each acoustic event recorded during fatigue tests. These two types of energy are compared in Fig. 16 for the three conditionings for a maximum applied stress of $\sigma_{max} = 0.6 \sigma_u$. The evolution of the normalized cumulative AE energy and of the hysteresis loop energy is plotted vs the number of fatigue cycles. Results show that the evolution of these two parameters are similar for each conditioning. For the Ambient one, both parameters have a slow progression during the first 98% of the fatigue life and an abrupt increase during the ultimate cycles (Fig. 16a). The evolution for the Wet/dry conditioning (Fig. 16c) is quite similar but with higher values of the hysteresis energy from the beginning of the test, which can be explained by the presence of a pre-damage, due to water desorption during the drying. The Wet conditioning (Fig. 16b) exhibits again a very different behaviour, with a significant increase in acoustic and hysteresis energy values during the first 30% of the fatigue life, then a plateau and finally an abrupt increase announcing the failure. These results demonstrate that these two different energy parameters exhibit globally the same trend during fatigue life for each conditioning, showing that the two corresponding techniques – acoustic emission and mechanical data recording – are able to reflect the same phenomenon, i.e. the damage development in the material.

3.4.2 Comparison of damage quantity obtained by micro-CT and mechanical parameters

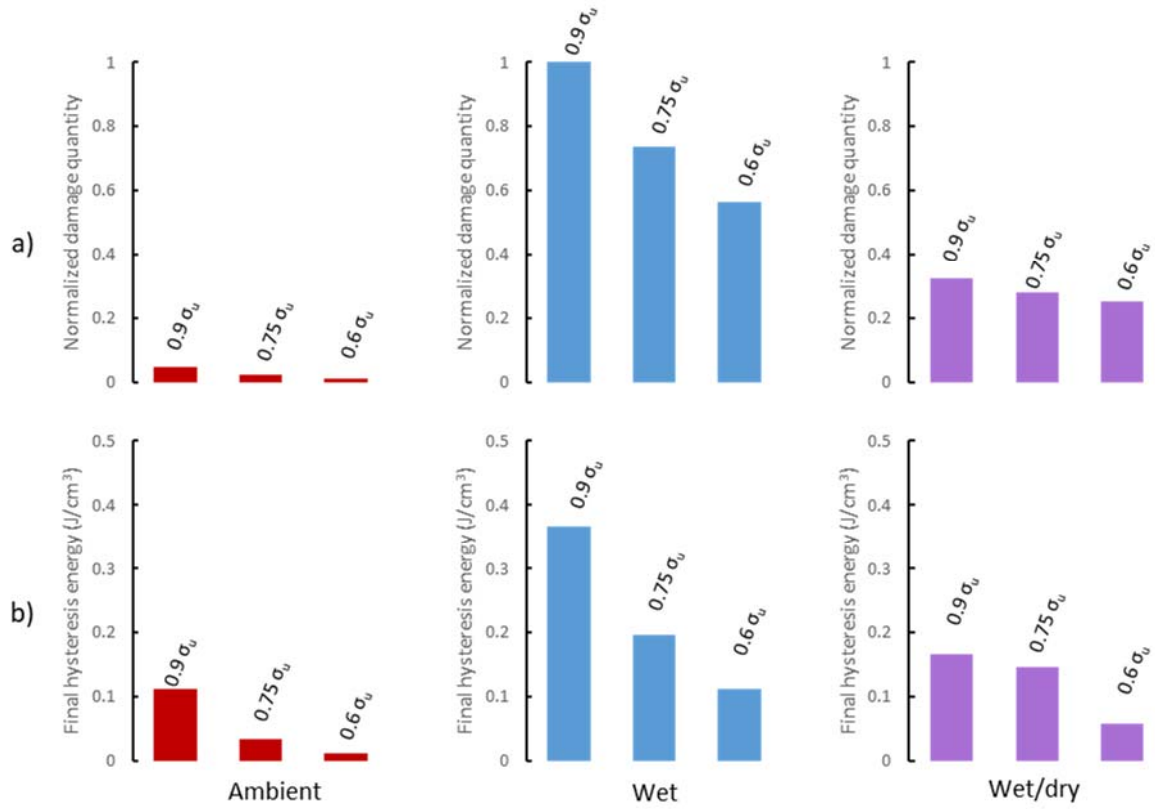


Fig. 17. Comparison of a) normalized damage quantity measured by micro-CT and b) final hysteresis energy for each level of maximum fatigue stress and each conditioning.

In order to compare the micro-CT results with the mechanical data, we have chosen to use the final value of hysteresis loop energy. Indeed, this value reflects the energy dissipated by the material just before failure, due to the damage that is present in the material at the end of the fatigue test. Therefore, we can compare it with the normalized damage quantity determined from the micro-CT scans performed after fatigue failure. Fig. 17 presents all the values obtained for the different conditionings and maximum fatigue stress levels. Results show that there is a great similarity between the evolutions of these two parameters depending on the conditioning and on the stress level. The higher the applied stress, the higher the values. For a given stress level, the Wet conditioning exhibits the highest values, then comes the Wet/dry conditioning and finally, with the lowest values, the Ambient conditioning. It confirms that the Wet conditioning is the most deteriorating condition for this plant fibre composite, the Wet/dry one having an intermediate behaviour between the Ambient and the Wet cases.

4. Conclusion

This study discusses the influence of moisture and drying on fatigue life and damage mechanisms for a woven [(±45)]₇ hemp/epoxy composite. The determination of the water absorption behaviour allowed to define the delay to reach saturation: 90 days. Therefore, three different conditionings have been applied: the Ambient one, with storage and testing in ambient environment, the Wet one, with water ageing from 90 to 100 days and testing at RH97, and the Wet/dry one, with a drying of 48h at 40°C after water ageing and then a mechanical testing in ambient environment. Thanks to tensile tests performed on samples for each conditioning, three levels of maximum fatigue stress were established: 60%, 75% and 90% of the tensile strength. All the fatigue tests were monitored with acoustic emission (AE) in order to compare the damage kinetics depending on the conditioning and on the applied stress level. AE data have been analysed through PCA (Principal Component Analysis) and k-means algorithm. Then, each AE cluster has been attributed to one particular damage mechanism: matrix cracking, interface damage or fibre breakage. After specimen failure, micro-CT scans have been performed on each specimen. The segmentation of grey levels in the reconstructed images allowed the determination of the relative damage volume. The comparison of mechanical data, i.e. fatigue hysteresis loop energy, with AE evolutions and micro-CT damage quantities demonstrates that these complementary techniques are all able to reflect the damage mechanisms occurring during fatigue testing.

The obtained results show that the Wet samples exhibit a lower tensile strength than the Ambient specimens and a lower fatigue sensitivity, while the behaviour of the Wet/dry samples is similar to the Wet conditioning one concerning the tensile strength and similar to the Ambient one concerning the fatigue sensitivity. The specific behaviour of the Wet/dry samples is directly linked with the deformation and damage mechanisms observed for this conditioning. Indeed, Wet/dry samples show an intermediate secant modulus decrease, an intermediate hysteresis loop energy level, an intermediate AE event evolution kinetics and an intermediate relative damage quantity. The Wet/dry specimens behave like pre-damaged Ambient specimens, that can be explained by the pre-damage created during the drying after the water ageing. Therefore, this study shows how the history of the specimen can have an influence on its fatigue properties: initial performances are not recovered after drying the sample.

Acknowledgements:

This work was partially funded by the French Government program “Investissements d’Avenir” (EQUIPEX GAP, reference ANR-11-EQPX-0018) and by the CPER FEDER project of Région Nouvelle Aquitaine.

References:

- [1] Witten, Elmar. European GRP market: the growth trend continued in 2018. Overview of the global composite market, vol. 127. JEC, Paris: 2019, p. 20–4.
- [2] Faruk O, Bledzki AK, Fink H-P, Sain M. Biocomposites reinforced with natural fibers: 2000–2010. *Progress in Polymer Science* 2012;37:1552–96. <https://doi.org/10.1016/j.progpolymsci.2012.04.003>.
- [3] Koronis G, Silva A, Fontul M. Green composites: A review of adequate materials for automotive applications. *Composites Part B: Engineering* 2013;44:120–7. <https://doi.org/10.1016/j.compositesb.2012.07.004>.
- [4] La Mantia FP, Morreale M. Green composites: A brief review. *Composites Part A: Applied Science and Manufacturing* 2011;42:579–88. <https://doi.org/10.1016/j.compositesa.2011.01.017>.
- [5] Shahzad A. Hemp fiber and its composites – a review. *Journal of Composite Materials* 2012;46:973–86. <https://doi.org/10.1177/0021998311413623>.
- [6] Manaia JP, Manaia AT, Rodrigues L. Industrial Hemp Fibers: An Overview. *Fibers* 2019;7:106. <https://doi.org/10.3390/fib7120106>.
- [7] Yashas Gowda TG, Sanjay MR, Subrahmanya Bhat K, Madhu P, Sentharamaikannan P, Yogesha B. Polymer matrix-natural fiber composites: An overview. *Cogent Engineering* 2018;5. <https://doi.org/10.1080/23311916.2018.1446667>.
- [8] Pitarresi G, Tumino D, Mancuso A. Thermo-Mechanical Behaviour of Flax-Fibre Reinforced Epoxy Laminates for Industrial Applications. *Materials* 2015;8:7371–88. <https://doi.org/10.3390/ma8115384>.
- [9] Mahboob Z, Bougherara H. Fatigue of flax-epoxy and other plant fibre composites: Critical review and analysis. *Composites Part A: Applied Science and Manufacturing* 2018;109:440–62. <https://doi.org/10.1016/j.compositesa.2018.03.034>.
- [10] Gholampour A, Ozbakkaloglu T. A review of natural fiber composites: properties, modification and processing techniques, characterization, applications. *J Mater Sci* 2020;55:829–92. <https://doi.org/10.1007/s10853-019-03990-y>.

- [11] Mejri M, Toubal L, Cuillière JC, François V. Hygrothermal aging effects on mechanical and fatigue behaviors of a short- natural-fiber-reinforced composite. *International Journal of Fatigue* 2018;108:96–108. <https://doi.org/10.1016/j.ijfatigue.2017.11.004>.
- [12] Fotouh A, Wolodko JD, Lipsett MG. Fatigue of natural fiber thermoplastic composites. *Composites Part B: Engineering* 2014;62:175–82. <https://doi.org/10.1016/j.compositesb.2014.02.023>.
- [13] Yuanjian T, Isaac DH. Impact and fatigue behaviour of hemp fibre composites. *Composites Science and Technology* 2007;67:3300–7. <https://doi.org/10.1016/j.compscitech.2007.03.039>.
- [14] Shahzad A, Isaac DH. Fatigue properties of hemp and glass fiber composites. *Polym Compos* 2014;35:1926–34. <https://doi.org/10.1002/pc.22851>.
- [15] de Vasconcellos DS, Touchard F, Chocinski-Arnault L. Tension–tension fatigue behaviour of woven hemp fibre reinforced epoxy composite: A multi-instrumented damage analysis. *International Journal of Fatigue* 2014;59:159–69. <https://doi.org/10.1016/j.ijfatigue.2013.08.029>.
- [16] Bensadoun F, Vallons KAM, Lessard LB, Verpoest I, Van Vuure AW. Fatigue behaviour assessment of flax–epoxy composites. *Composites Part A: Applied Science and Manufacturing* 2016;82:253–66. <https://doi.org/10.1016/j.compositesa.2015.11.003>.
- [17] Liang S, Gning PB, Guillaumat L. A comparative study of fatigue behaviour of flax/epoxy and glass/epoxy composites. *Composites Science and Technology* 2012;72:535–43. <https://doi.org/10.1016/j.compscitech.2012.01.011>.
- [18] Doan T-T-L, Brodowsky H, Mäder E. Jute fibre/epoxy composites: Surface properties and interfacial adhesion. *Composites Science and Technology* 2012;72:1160–6. <https://doi.org/10.1016/j.compscitech.2012.03.025>.
- [19] Huber T, Pang S, Staiger MP. All-cellulose composite laminates. *Composites Part A: Applied Science and Manufacturing* 2012;43:1738–45. <https://doi.org/10.1016/j.compositesa.2012.04.017>.
- [20] Muñoz E, García-Manrique JA. Water Absorption Behaviour and Its Effect on the Mechanical Properties of Flax Fibre Reinforced Bioepoxy Composites. *International Journal of Polymer Science* 2015;2015:1–10. <https://doi.org/10.1155/2015/390275>.
- [21] Assarar M, Scida D, El Mahi A, Poilâne C, Ayad R. Influence of water ageing on mechanical properties and damage events of two reinforced composite materials: Flax–fibres and glass–fibres. *Materials & Design* 2011;32:788–95. <https://doi.org/10.1016/j.matdes.2010.07.024>.

- [22] Maslinda AB, Abdul Majid MS, Ridzuan MJM, Afendi M, Gibson AG. Effect of water absorption on the mechanical properties of hybrid interwoven cellulosic-cellulosic fibre reinforced epoxy composites. *Composite Structures* 2017;167:227–37. <https://doi.org/10.1016/j.compstruct.2017.02.023>.
- [23] Perrier A, Touchard F, Chocinski-Arnault L, Mellier D. Influence of water on damage and mechanical behaviour of single hemp yarn composites. *Polymer Testing* 2017;57:17–25. <https://doi.org/10.1016/j.polymertesting.2016.10.035>.
- [24] Bouchak M, Farrow I, Bond I, Rowland C, Menan F. Acoustic emission energy as a fatigue damage parameter for CFRP composites. *International Journal of Fatigue* 2007;29:457–70. <https://doi.org/10.1016/j.ijfatigue.2006.05.009>.
- [25] Unnthorsson R, Runarsson T, Jonsson M. Acoustic emission based fatigue failure criterion for CFRP. *International Journal of Fatigue* 2008;30:11–20. <https://doi.org/10.1016/j.ijfatigue.2007.02.024>.
- [26] Maillet E, Baker C, Morscher GN, Pujar VV, Lemanski JR. Feasibility and limitations of damage identification in composite materials using acoustic emission. *Composites Part A: Applied Science and Manufacturing* 2015;75:77–83. <https://doi.org/10.1016/j.compositesa.2015.05.003>.
- [27] Madra A, Adrien J, Breitkopf P, Maire E, Trochu F. A clustering method for analysis of morphology of short natural fibers in composites based on X-ray microtomography. *Composites Part A: Applied Science and Manufacturing* 2017;102:184–95. <https://doi.org/10.1016/j.compositesa.2017.07.028>.
- [28] Perrier A, Touchard F, Chocinski-Arnault L, Mellier D. Quantitative analysis by micro-CT of damage during tensile test in a woven hemp/epoxy composite after water ageing. *Composites Part A: Applied Science and Manufacturing* 2017;102:18–27. <https://doi.org/10.1016/j.compositesa.2017.07.018>.
- [29] Ben Ameer M, El Mahi A, Rebiere J-L, Gimenez I, Beyaoui M, Abdennadher M, et al. Investigation and identification of damage mechanisms of unidirectional carbon/flax hybrid composites using acoustic emission. *Engineering Fracture Mechanics* 2019;216:106511. <https://doi.org/10.1016/j.engfracmech.2019.106511>.
- [30] Jani SP, Kumar AS, Khan MA, Sajith S, Saravanan A. Influence of Natural Filler on Mechanical Properties of Hemp/Kevlar Hybrid Green Composite and Analysis of Change in Material Behavior Using Acoustic Emission. *Journal of Natural Fibers* 2019:1–12. <https://doi.org/10.1080/15440478.2019.1692321>.
- [31] El Mahi A, Daoud H, Rebiere J-L, Gimenez I, Taktak M, Haddar M. Damage mechanisms characterization of flax fibers–reinforced composites with interleaved natural viscoelastic layer using

- acoustic emission analysis. *Journal of Composite Materials* 2019;53:2623–37.
<https://doi.org/10.1177/0021998319836236>.
- [32] Piech. CS221 2013. <https://stanford.edu/~cpiech/cs221/handouts/kmeans.html> (accessed July 25, 2019).
- [33] Assarar M, Scida D, Zouari W, Saidane EH, Ayad R. Acoustic emission characterization of damage in short hemp-fiber-reinforced polypropylene composites. *Polym Compos* 2016;37:1101–12.
<https://doi.org/10.1002/pc.23272>.
- [34] Marec A, Thomas J-H, El Guerjouma R. Damage characterization of polymer-based composite materials: Multivariable analysis and wavelet transform for clustering acoustic emission data. *Mechanical Systems and Signal Processing* 2008;22:1441–64. <https://doi.org/10.1016/j.ymssp.2007.11.029>.
- [35] Li L, Lomov SV, Yan X, Carvelli V. Cluster analysis of acoustic emission signals for 2D and 3D woven glass/epoxy composites. *Composite Structures* 2014;116:286–99.
<https://doi.org/10.1016/j.compstruct.2014.05.023>.
- [36] Li L, Swolfs Y, Straumit I, Yan X, Lomov SV. Cluster analysis of acoustic emission signals for 2D and 3D woven carbon fiber/epoxy composites. *Journal of Composite Materials* 2016;50:1921–35.
<https://doi.org/10.1177/0021998315597742>.
- [37] Fujii T, Amijima S, Okubo K. Microscopic fatigue processes in a plain-weave glass-fibre composite. *Composites Science and Technology* 1993;49:327–33. [https://doi.org/10.1016/0266-3538\(93\)90063-M](https://doi.org/10.1016/0266-3538(93)90063-M).
- [38] Pandita SD, Huysmans G, Wevers M, Verpoest I. Tensile fatigue behaviour of glass plain-weave fabric composites in on- and off-axis directions. *Composites Part A: Applied Science and Manufacturing* 2001;32:1533–9. [https://doi.org/10.1016/S1359-835X\(01\)00053-7](https://doi.org/10.1016/S1359-835X(01)00053-7).
- [39] Daggumati S, De Baere I, Van Paepegem W, Degrieck J, Xu J, Lomov SV, et al. Local damage in a 5-harness satin weave composite under static tension: Part I – Experimental analysis. *Composites Science and Technology* 2010;70:1926–33. <https://doi.org/10.1016/j.compscitech.2010.07.003>.
- [40] Osada T, Mizoguchi M, Kotaki M. Initial micro fracture behavior of woven fabric composites. ICCM13, Beijing (China), 2001, p. ID1083.
- [41] Godin N, Reynaud P, Fantozzi G. Challenges and Limitations in the Identification of Acoustic Emission Signature of Damage Mechanisms in Composites Materials. *Applied Sciences* 2018;8:1267.
<https://doi.org/10.3390/app8081267>.
- [42] Shen C-H, Springer GS. Moisture Absorption and Desorption of Composite Materials. *Journal of Composite Materials* 1976;10:2–20. <https://doi.org/10.1177/002199837601000101>.

- [43] Kanny K, T.P. M. Surface treatment of sisal fiber composites for improved moisture and fatigue properties. *Composite Interfaces* 2013;20:783–97. <https://doi.org/10.1080/15685543.2013.819699>.
- [44] Ventura H, Claramunt J, Rodríguez-Pérez MA, Ardanuy M. Effects of hydrothermal aging on the water uptake and tensile properties of PHB/flax fabric biocomposites. *Polymer Degradation and Stability* 2017;142:129–38. <https://doi.org/10.1016/j.polymdegradstab.2017.06.003>.
- [45] Thwe MM, Liao K. Effects of environmental aging on the mechanical properties of bamboo–glass fiber reinforced polymer matrix hybrid composites. *Composites Part A: Applied Science and Manufacturing* 2002;33:43–52. [https://doi.org/10.1016/S1359-835X\(01\)00071-9](https://doi.org/10.1016/S1359-835X(01)00071-9).
- [46] Barbosa JF, Correia JA, Freire Júnior R, Zhu S-P, De Jesus AM. Probabilistic S-N fields based on statistical distributions applied to metallic and composite materials: State of the art. *Advances in Mechanical Engineering* 2019;11:168781401987039. <https://doi.org/10.1177/1687814019870395>.
- [47] Diniz B da C, Freire Júnior RCS. Study of the fatigue behavior of composites using modular ANN with the incorporation of a posteriori failure probability. *International Journal of Fatigue* 2020;131:105357. <https://doi.org/10.1016/j.ijfatigue.2019.105357>.
- [48] Zhou S, Wu X. Fatigue life prediction of composite laminates by fatigue master curves. *Journal of Materials Research and Technology* 2019;8:6094–105. <https://doi.org/10.1016/j.jmrt.2019.10.003>.
- [49] Huang J, Pastor ML, Garnier C, Gong XJ. A new model for fatigue life prediction based on infrared thermography and degradation process for CFRP composite laminates. *International Journal of Fatigue* 2019;120:87–95. <https://doi.org/10.1016/j.ijfatigue.2018.11.002>.
- [50] Zhang W, Jiang T, Liu L. Low Cycle Fatigue Life Prediction Model of 800H Alloy Based on the Total Strain Energy Density Method. *Materials* 2019;13:76. <https://doi.org/10.3390/ma13010076>.
- [51] Epaarachchi JA, Clausen PD. An empirical model for fatigue behavior prediction of glass fibre-reinforced plastic composites for various stress ratios and test frequencies. *Composites Part A: Applied Science and Manufacturing* 2003;34:313–26. [https://doi.org/10.1016/S1359-835X\(03\)00052-6](https://doi.org/10.1016/S1359-835X(03)00052-6).
- [52] Caprino G, D'Amore A. Flexural fatigue behaviour of random continuous-fibre-reinforced thermoplastic composites. *Composites Science and Technology* 1998;58:957–65. [https://doi.org/10.1016/S0266-3538\(97\)00221-2](https://doi.org/10.1016/S0266-3538(97)00221-2).
- [53] D'Amore A, Caprino G, Nicolais L, Marino G. Long-term behaviour of PEI and PEI-based composites subjected to physical aging. *Composites Science and Technology* 1999;59:1993–2003. [https://doi.org/10.1016/S0266-3538\(99\)00058-5](https://doi.org/10.1016/S0266-3538(99)00058-5).

- [54] Jeannin T, Berges M, Gabrion X, Léger R, Person V, Corn S, et al. Influence of hydrothermal ageing on the fatigue behaviour of a unidirectional flax-epoxy laminate. *Composites Part B: Engineering* 2019;174:107056. <https://doi.org/10.1016/j.compositesb.2019.107056>.
- [55] Van Paepegem W. A new coupled approach of residual stiffness and strength for fatigue of fibre-reinforced composites. *International Journal of Fatigue* 2002;24:747–62. [https://doi.org/10.1016/S0142-1123\(01\)00194-3](https://doi.org/10.1016/S0142-1123(01)00194-3).
- [56] Malpot A, Touchard F, Bergamo S. Influence of moisture on the fatigue behaviour of a woven thermoplastic composite used for automotive application. *Materials & Design* 2016;98:12–9. <https://doi.org/10.1016/j.matdes.2016.02.123>.
- [57] Huelsbusch D, Jamrozy M, Frieling G, Mueller Y, Barandun GA, Niedermeier M, et al. Comparative characterization of quasi-static and cyclic deformation behavior of glass fiber-reinforced polyurethane (GFR-PU) and epoxy (GFR-EP). *Materials Testing* 2017;59:109–17. <https://doi.org/10.3139/120.110972>.
- [58] Perrier A, Le Bourhis E, Touchard F, Chocinski-Arnault L. Effect of water ageing on nanoindentation response of single hemp yarn/epoxy composites. *Composites Part A: Applied Science and Manufacturing* 2016;84:216–23. <https://doi.org/10.1016/j.compositesa.2016.01.022>.
- [59] de Miguel AG, Pagani A, Carrera E. Free-edge stress fields in generic laminated composites via higher-order kinematics. *Composites Part B: Engineering* 2019;168:375–86. <https://doi.org/10.1016/j.compositesb.2019.03.047>.
- [60] Lecomte-Grosbras P, Paluch B, Brieu M. Characterization of free edge effects: influence of mechanical properties, microstructure and structure effects. *Journal of Composite Materials* 2013;47:2823–34. <https://doi.org/10.1177/0021998312458817>.